arXiv:astro-ph/0506331v1 15 Jun 2005

Chandra Observations of A Galactic Supernova Remnant Vela Jr.: A New Sample of Thin Filaments Emitting Synchrotron X-Rays

Aya Bamba[1], Ryo Yamazaki[2], Junko S. Hiraga[3]

bamba@crab.riken.jp, ryo@vega.ess.sci.osaka-u.ac.jp,
jhiraga@astro.isas.jaxa.jp

ABSTRACT

A galactic supernova remnant (SNR) Vela Jr. (RX J0852.0−4622, G266.6−1.2) shows sharp filamentary structure on the north-western edge of the remnant in the hard X-ray band. The filaments are so smooth and located on the most outer side of the remnant. We measured the averaged scale width of the filaments (w_u and w_d) with excellent spatial resolution of *Chandra*, which are in the order of the size of the point spread function of *Chandra* on the upstream side and 49.5 (36.0–88.8) arcsec on the downstream side, respectively. The spectra of the filaments are very hard and have no line-like structure, and were well reproduced with an absorbed power-law model with Γ =2.67 (2.55–2.77), or a `SRCUT` model with $\nu_{rolloff}$ = 4.3 (3.4–5.3)$\times 10^{16}$ Hz under the assumption of $p = 0.3$. These results imply that the hard X-rays are synchrotron radiation emitted by accelerated electrons, as mentioned previously. Using a correlation between a function $\mathcal{B} \equiv \nu_{rolloff}/w_d^2$ and the SNR age, we estimated the distance and the age of Vela Jr.: the estimated distance and age are 0.33 (0.26–0.50) kpc and 660 (420–1400) years, respectively. These results are consistent with previous reports, implying that $\mathcal{B}$–age relation may be a useful tool to estimate the distance and the age of synchrotron X-ray emitting SNRs.

Subject headings: acceleration of particles — supernova remnants: individual (Vela Jr.) — X-rays: ISM

[1]RIKEN (The Institute of Physical and Chemical Research) 2-1, Hirosawa, Wako, Saitama 351-0198, Japan

[2]Department of Earth and Space Science, Graduate School of Science, Osaka University, Toyonaka, Osaka 560-0043, Japan

[3]Department of High Energy Astrophysics Institute of Space and Astronautical Science (ISAS) Japan Aerospace Exploration Agency (JAXA) 3-1-1 Yoshinodai, Sagamihara, Kanagawa 229-8510, Japan

1. Introduction

Supernova remnants (SNRs) play crucial roles for heating and chemical evolution of galaxies. Their shocks are also famous as cosmic-ray accelerators. Koyama et al. (1995) discovered synchrotron X-rays from shells of SN 1006, which is the first observational result indicating that SNRs accelerate electrons up to ∼TeV. At present, several SNRs have been identified as synchrotron X-ray emitters (e.g. RX J1713.7−3946, Koyama et al. 1997; Slane et al. 1999; RCW 86, Bamba, Tomida, & Koyama 2000; Borkowski et al. 2001; Rho et al. 2002; Cas A., Vink & Laming 2003; see also Bamba et al. 2005; Bamba 2004).

The most plausible acceleration mechanism is the diffusive shock acceleration (DSA) (e.g. Bell 1978; Drury 1983; Blandford & Eichler 1987; Jones & Ellison 1991; Malkov & Drury 2001), which can accelerate charged particles on the shock into a power-law distribution, similar to the observed spectrum of cosmic rays on the earth. However, since there is still little observational information and theoretical understanding, there are many unresolved problems, such as the injection efficiency, the maximum energy of accelerated particles, the configurations of magnetic field, and so on. The magnetic field amplification is also pointed out as an remarkable process (Bell & Lucek 2001; Lucek & Bell 2000). Recently, it is found that nonthermal X-rays from the shells of historical SNRs concentrate on very narrow filamentary regions (Bamba et al. 2003b, 2005). Together with the roll-off frequency ($\nu_{rolloff}$) of synchrotron X-rays (Reynolds 1998; Reynolds & Keohane 1999), Bamba et al. (2005) found that an empirical function, $\mathcal{B} \equiv \nu_{rolloff}/{w_d}^2$, decreases with the age of an SNR ($\mathcal{B}$—age relation). The relation may reflect the time evolution of the magnetic field around the shock front (Bamba et al. 2005). However, the $\mathcal{B}$—age relation has still many uncertainties because of poor statistics. Clearly other new samples with synchrotron X-ray filaments are desired.

Vela Jr. (RX J0852.0−4622, G266.6−1.2) is one of the most curious galactic SNR with large radius of about 60 arcmin (Green 2004). It was discovered by *ROSAT* (Aschenbach 1998). and well known that the *COMPTEL* team reported a possible detection of 1.157 MeV γ-ray line emitted by ^{44}Ti (Iyudin et al. 1998). This fact strongly indicates that Vela Jr. is a nearby and very young SNR because the half lifetime of ^{44}Ti is only about 60 years, however, there remains some doubt about the detection (Shonfelder et al. 2000). Tsunemi et al. (2000) reported the presence of Ca K line, suggesting that there are a plenty of Ca produced from ^{44}Ti. On the other hand, Slane et al. (2001) reported that the 1σ upper-limit of Sc-K line is 4.4×10^{-6} cm^{-2}s^{-1}. Recently, Iyudin et al. (2005) found the possible detection of Ti and Sc K emission lines with *XMM-Newton*. For the 78.4 keV line emission from ^{44}Ti, von Keinlin et al. (2004) obtained the upper-limit of 1.1×10^{-4} cm^{-2}s^{-1} with *INTEGRAL*/SPI. The presence of a central source has been also suggested (Aschenbach

1998), which was confirmed with *Chandra* (Pavlov et al. 2001). The spectrum of the source, CXOU J085201.4−461753, together with the absence of any optical counter part (Mereghetti, Pellizzoni, & de Luca 2002), reminds us of a neutron star. These observational reports might indicate that the progenitor is a core-collapse supernova (SN).

The other fact which makes this SNR famous is the existence of nonthermal X-rays from the rims (Slane et al. 2001), which implies that the rims of Vela Jr. are cosmic ray accelerators like SN 1006 (Koyama et al. 1995) and other SNRs with synchrotron X-rays (e.g. Bamba 2004, and references therein). Recently, TeV γ-rays with energies greater than 500 GeV are also detected at the 6σ level from the north-western rim of the SNR with *CANGAROO-II* (Katagiri et al. 2005) and H.E.S.S. (Aharonian et al. 2005). These γ-rays are produced by accelerated electrons and/or protons with energies more than $\sim$ TeV.

Despite such an interesting source, the precise age of the remnant is still unknown. There are some spikes in nitrate concentration measured in an Antarctic ice core, which might be regarded as signals of SNe (Burgess & Zuber 2000). One of them is not yet identified with historical SNe ever known. If the spike really associated with the progenitor of Vela Jr., the SN may have occurred around AD 1320 and the age of the remnant is about 680 yrs. However, there are many uncertainties, hence further studies are necessary. In addition, an unclear issue is the distance to the remnant, which brings us numerous information, such as the total luminosity of the ^{44}Ti emission line, the average expansion velocity, and so on. It may also give us some answer on the current debate whether or not Vela (the distance of 250 pc; Cha et al. 1999) and Vela Jr. interact with each other. Iyudin et al. (1998) estimated the distance to be $\sim$200 pc with an assumption that the age is 680 years mentioned above, while Slane et al. (2001) suggested that the distance is 1–2 kpc from the relatively large absorption column. Although Moriguchi et al. (2001) observed the molecular distribution using ^{12}CO (J = 1—0) emission with NANTEN, they could not determine the precise distance because the remnant is located near the tangential point of a galactic arm. The upper limit of the distance they estimated is $\sim$1 kpc.

In this paper, using the *Chandra* data for the first time, we report on the analysis of hard X-ray filaments associated with Vela Jr. and discuss on the acceleration mechanism at the shock of the SNR, its age, and the distance to the SNR. This paper is organized as follows. We summarize the observation details of Vela Jr. with *Chandra* in § 2. Section 3 describes the results of the observations. We discuss on ^{44}Sc emission line reported by Iyudin et al. (2005) in § 4, the origin of nonthermal X-rays in § 5, on the interaction between the SNR and molecular clouds (§ 6), and on the origin of TeV γ-rays (§ 7). In § 8, we argue the distance and the age of the SNR using the correlation between a function $\mathcal{B}$ and the SNR age.

2. Observations

We used the *Chandra* archival data of the ACIS of the north-western (NW) rim of Vela Jr. (ObsID = 3846 and 4414). Figure 1 shows the *ASCA* GIS image (Tsunemi et al. 2000) with the field of view of *Chandra* observations. The satellite and the instrument are described by Weisskopf et al. (2002) and Garmire et al. (2000), respectively. Data acquisition from the ACIS was made in the Timed-Exposure Faint mode. The data reductions and analysis were made using the *Chandra* Interactive Analysis of Observations (CIAO) software version 3.0.2. Using the Level 2 processed events provided by the pipeline processing at the *Chandra* X-ray Center, we selected *ASCA* grades 0, 2, 3, 4, and 6, as the X-ray events. The "streak" events on the CCD chip S4 were removed by using the program *destreak*[1] in CIAO. In order to make statistics better, we improved the astrometory of the data following the CIAO data analysis threads and combined these data. The exposure time of each observation is 39 ks (ObsID = 3846) and 35 ks (ObsID = 4414), respectively. Table 1 summarizes about these observations. Hereinafter, all results are from the combined data so far as there is no mention.

3. Results

Figure 2 shows images of the NW rim in the 0.5–2.0 keV (a) and 2.0–10.0 keV (b) bands, binned with 4 arcsec scale. Neither the subtraction of background photons, smoothing process, nor correction of the exposure time did not be performed. The difference of background level among the chips are caused by that of the CCD chips (back-illuminated and front-illuminated). These images look alike, and show very straight filamentary structures clearly on the outer edge of the rim. Two filaments can be well recognized especially in the upper panel. Iyudin et al. (2005) suggests that the inner filament may be the reverse shock emission. However, we have no clue to distinguish whether it indicates the reverse shock or apparently overlaid forward shock via the projection effect. The filaments are very similar to those in SN 1006 (Long et al. 2003; Bamba et al. 2003b), indicating that they may be efficient accelerators of electrons like SN 1006 filaments. Then we made analysis in the same way to our previous one for SN 1006 (Bamba et al. 2003b).

For the first step, we made a spectrum from the whole emitting region of this rim. Since the rim is covered by two CCD chips (chip 6 and 7), source spectra were made separately from each chip. Background photons were accumulated from outer regions of the rim. All the spectra extend up to >2 keV, indicating that the hard X-ray emission is nonthermal.

[1]See http://asc.harvard.edu/ciao2.3/ahelp/destreak.html.

There is some line-like feature below 2 keV, which probably comes from thermal emission of Vela and/or Vela Jr. as already mentioned (Slane et al. 2001). Since our data does not have sufficient statistics to examine the properties of thermal plasma, we ignored the component. In Hiraga et al. (2005), detailed analysis for the thermal plasma is done with the *XMM-Newton* deep observation. We fitted the spectra with an absorbed power-law model only with photons above 2 keV, in order to avoid the contamination of thermal photons. The absorption column was subsequently calculated using the cross sections by Morrison & McCammon (1983) with the solar abundances (Anders & Grevesse 1989). The best-fit parameters are shown in Table 2.

The best-fit values of the photon index and absorption column are consistent with those of the nonthermal component in previous results (Slane et al. 2001; Iyudin et al. 2005; Hiraga et al. 2005), indicating that almost all photons above 2 keV are nonthermal origin. Thus, we regarded all the photons above 2 keV as nonthermal in the following. As shown in Figure 2(b), three filaments were selected (filament 1–3) in order to study their spatial and spectral characteristics, which are straight and free from other structures, in the same way to the analysis of SN 1006 case (Bamba et al. 2003b). Since all the filaments are located within 4 arcmin from the aim-point (see Table 1), the size of a point spread function (PSF) is about 0.5 arcsec. Although we can see the filaments more clearly in the soft X-ray band in Figure 2, Bamba et al. (2003b) showed us that the contamination of thermal photons makes filaments broader. Therefore, we conducted the spatial analysis only with photons above 2 keV. Figure 3 shows spatial profiles of the filaments in the 2.0–10.0 keV (nonthermal) band binned to a resolution of 1 arcsec. We can see profiles with clear decays on the downstream sides and sharp edges on the upstream sides in all profiles. The filament 2 and 3 are double peaked, as suggested by Iyudin et al. (2005). To estimate the scale width of these filaments on upstream (w_u) and downstream (w_d) sides, we fitted them with exponential function as a simple and empirical fitting model for the apparent profiles, which is the same as used in the previous analysis in the SN 1006 (Bamba et al. 2003b) and other historical SNR (Bamba et al. 2005) cases. Background photons were not subtracted and treated as a spatially independent component. For the filament 3, the w_u could not be determined due to the lack of statistics, then it was frozen to be the PSF size (0.5 arcsec). For each filament, fitting region was limited around the outermost peak in order to avoid the influence of the inner structure. The model well reproduced the data. The best-fit models and parameters are shown in Figure 3 and Table 3, respectively.

For the next step, we made spectra of the filaments. The background regions were selected from the downstream sides of the filaments, where there was no other structure. The spectra were so hard and fitted with an absorbed power-law model again. The absorption column was fixed to be 6.1×10^{21} cm^{-2} in order to make statistics better, which is the best-fit

value for the total region (Table 2) and consistent with previous results. The index of the power-law component is similar to those of nonthermal shells in other SNRs (SN 1006, Bamba et al. 2003b; RX J1713.7−3946, Koyama et al. 1997; Slane et al. 1999), which is considered to be synchrotron emission. Therefore, we concluded that the nonthermal emission in Vela Jr. shell is synchrotron, and applied the `SRCUT` model, which is one of the model representing the synchrotron emission from electrons of power-law distribution with exponential roll-off in a homogeneous magnetic field (Reynolds 1998; Reynolds & Keohane 1999). The spectral index at 1 GHz was fixed to be 0.3 according to a report by Combi, Romero, & Benaglia (1999). Since the value $p = 0.3$ is rather smaller than those of ordinary SNRs, about 0.5, we also tested the model under the assumption of $p = 0.5$. All models can reproduce the data with similar values of reduced χ^2 as shown in Table 4.

4. Comments on ^{44}Sc fluorescent line

Iyudin et al. (2005) reported a significant emission line at 4.45±0.05 keV from the NW rim of Vela Jr. with *XMM-Newton*. We checked the spectrum of each filament as well as the averaged one so as to investigate the presence of some line-like feature. As a result, we found that the spectrum of filament 1 has an excess around 4 keV as shown in Figure 4, while the spectrum averaged for whole rim does not show the line feature. Since one can see the excess in the data of both observations, it may be a real line. Then, the power-law plus a narrow line model were applied and accepted, although the reduced χ^2 does not improve significantly (χ^2/d.o.f.=69.5/79; see also Table 4). The center energy is 4.1 ± 0.2 keV, which is slightly lower than the averaged one by Iyudin et al. (2005) but consistent with the *ASCA* result (Tsunemi et al. 2000). The total flux, $7.3^{+5.1}_{-4.5} \times 10^{-7}$ photons cm^{-2}s^{-1}, is about 10% of that derived by Iyudin et al. (2005) and Tsunemi et al. (2000), and consistent with the upper limit by Slane et al. (2001). The difference of the intensity may be because of our smaller region the spectra were accumulated than those by other authors. Moreover, the center energy and significance depend on the choice of the background region and the model of the continuum component. The lack of statistics prevents us from reliable conclusion. Detailed analysis with excellent statistics and spectral resolution are encouraged.

5. Origin of the Filaments

We found that the scale width of the filaments in Vela Jr. is much smaller than its radius. Filament 3 has a small w_u in the order of *Chandra* PSF size (0.5 arcsec), indicating that the w_u may be similar to or smaller than the PSF size. Although the other filaments

have w_u significantly larger than the PSF size, it may be caused by the projection effect or other structures, such as the second peak and/or other filaments. Therefore, we concluded that the scale width on the upstream side is similar to or smaller than the PSF size. On the other hand, the value of w_d is much larger than the PSF size. These results are similar to other case of nonthermal filaments in young SNRs (Bamba et al. 2005). The power-law index is similar to the results with previous observations (Slane et al. 2001; Hiraga et al. 2005). These thin filaments with hard X-rays remind us the nonthermal X-rays from filaments in young SNRs. Wide band spectra of most of these SNRs show that the nonthermal X-rays are synchrotron radiation from highly accelerated electrons. Therefore, we consider that the filaments emit X-rays via synchrotron radiation. In order to confirm our conclusion, we need more information in the radio continuum band to make the wide band spectrum of synchrotron emission.

6. Interaction with Molecular Clouds?

The filaments in Vela Jr. are rather straight and their lengths are comparable to the radius of the SNR, that are similar to those in SN 1006 (Bamba et al. 2003b) and Tycho (Hwang et al. 2002), and are unlike clumpy filaments in Cas A (Vink & Laming 2003), RCW 86 (Rho et al. 2002), and RX J1713.7−3946 (Uchiyama et al. 2003; Lazendic et al. 2004; Cassam-Chenaï et al. 2004). The former samples are located in tenuous interstellar space, whereas for the two SNRs in the latter cases, there are some reports about the interaction between shocks and molecular clouds (RCW 86: Moriguchi et al., private communication; RX J1713.7−3946: Fukui et al. 2003). Interactions with molecular clouds may distort beautiful filaments via turbulence and so on. There are molecular clouds around Vela Jr. (Moriguchi et al. 2001). However, it is not clear whether the shocks are interacting with them or not, because there is no observation with excited molecular cloud lines (CO(2→1) and so on). The straight filaments may indicate that there is no interaction between the shock and the molecular cloud in this region. Further observations with excited molecular lines are needed.

7. Origin of TeV γ-rays

Recently, two instruments have independently detected TeV γ-rays significantly (Katagiri et al. 2005; Aharonian et al. 2005). The reported differential flux is consistent with each other, but the photon index is slightly different. In this section, we examine the origin of the TeV γ-rays, considering the preferable values of the maximum energy of electrons (E_{max})

and the downstream magnetic field (B_d) (Yamazaki et al. 2004). Bamba et al. (2005) suggested that the width of the filament on the downstream side (w_d) and the roll-off frequency of synchrotron emission ($\nu_{rolloff}$) reflect the value of E_{max} and B_d, then we can use these two observational value for the study on E_{max} and B_d. Hereinafter, we adopt flux-averaged mean values, such as

$$w_d = 49.5 \text{ arcsec} = 0.24^{+0.19}_{-0.07} \left(\frac{D}{1 \text{ kpc}}\right) \text{ pc} \quad , \tag{1}$$

$$\nu_{rolloff} = 6.6^{+2.1}_{-1.6} \times 10^{16} \text{ Hz} \quad , \tag{2}$$

where D is the distance to Vela Jr. Considering the projection effect, w_d can be written as

$$\begin{aligned} w_d &= \alpha r^{-1} u_s t_{loss} \quad , \\ t_{loss} &= 1.25 \times 10^3 \text{ yrs} \left(\frac{E_{max}}{100 \text{ TeV}}\right)^{-1} \left(\frac{B_d}{10\ \mu\text{G}}\right)^{-2} \quad , \end{aligned}$$

where α, r, u_s, and t_{loss} are a correction factor of the projection effect, the compression ratio, the shock velocity, and synchrotron loss time scale (Bamba et al. 2005; Yamazaki et al. 2004). Although α is an unknown parameter depending on the shape of profiles and the curvature radius, it becomes ∼1–10 as far as the width of filaments is negligible to the SNR radii (Berezhko & Völk 2004). Then the above equations lead

$$\left(\frac{E_{max}}{100 \text{ TeV}}\right)^{-1} \left(\frac{B_d}{10\ \mu\text{G}}\right)^{-2} = 6.3^{+5.0}_{-1.8} \times 10^{-2} \alpha^{-1} r \left(\frac{u_s}{3000 \text{ km s}^{-1}}\right)^{-1} \left(\frac{D}{1 \text{ kpc}}\right) \quad . \tag{3}$$

On the other hand, the roll-off frequency $\nu_{rolloff}$ is represented as (Reynolds & Keohane 1999; Reynolds 1998)[2]

$$\nu_{rolloff} = 1.6 \times 10^{18} \text{ Hz} \left(\frac{E_{max}}{100 \text{ TeV}}\right)^2 \left(\frac{B_d}{10\ \mu\text{G}}\right) \quad . \tag{4}$$

In the following, we adopt typical values $\alpha = 5$ and $r = 4$. Then, using Eqs. (3) and (4), we derived

$$E_{max} = 4.1^{+0.9}_{-0.9} \text{ TeV} \left(\frac{u_s}{3000 \text{ km s}^{-1}}\right)^{-1/3} \left(\frac{D}{1 \text{ kpc}}\right)^{1/3} \left(\frac{\alpha}{5}\right)^{-1/3} \left(\frac{r}{4}\right)^{1/3} \quad , \tag{5}$$

$$B_d = 2.2^{+0.2}_{-0.2} \times 10^2\ \mu\text{G} \left(\frac{u_s}{3000 \text{ km s}^{-1}}\right)^{2/3} \left(\frac{D}{1 \text{ kpc}}\right)^{-2/3} \left(\frac{\alpha}{5}\right)^{2/3} \left(\frac{r}{4}\right)^{-2/3} \quad . \tag{6}$$

[2]See http://heasac.gsfc.nasa.gov/docs/xanadu/xspec for the erratum of coefficients.

Katagiri et al. (2005) examined whether the TeV γ-rays arise from the inverse Compton emission via accelerated electrons or π^0 decay caused by accelerated protons. The former requires very high size ratio of X-ray and TeV γ-ray emission regions ($V_{\rm TeV}/V_{\rm X-ray} \sim 10^5$) and strong magnetic field of B_d ∼1.6 mG. Then we obtain the shock velocity with eq.(6) as

$$u_s \sim 6 \times 10^8 \text{ cm s}^{-1} \left(\frac{D}{100 \text{ pc}}\right) \left(\frac{\alpha}{5}\right)^{-1} \left(\frac{r}{4}\right) \quad , \tag{7}$$

so that the small distance, $D \lesssim 100$ pc (the very small physical radius and the very young age, in other words) may be required, which is somewhat doubtful. This result is consistent with the discussion in Aharonian et al. (2005). On the other hand, π^0-decay model, which requires the interaction of the SNR and molecular clouds, can naturally explain the multi-band spectrum (Katagiri et al. 2005). However, there might be some discrepancy between the observed straight filaments as discussed in § 6.

8. Estimation of the Age and the Distance

More determinative arguments on the distance (D) can be possible, and at this time, the age of the SNR (t_{age}) can be also discussed simultaneously. As a tool of the estimation, $\mathcal{B}$—age relation (Bamba et al. 2005) is used, where

$$\mathcal{B} \equiv \nu_{rolloff}/{w_d}^2 = C{t_{age}}^{\alpha} \quad , \tag{8}$$

$$C = 2.6^{+1.2}_{-1.4} \times 10^{27} \text{ Hzpc}^{-2}, \tag{9}$$

$$\alpha = -2.96^{+0.11}_{-0.06} \quad . \tag{10}$$

Let θ_R ($\equiv R_s/D$) and θ_d ($\equiv w_d/D$) be the angular radius of the SNR and the observed angular scale width of synchrotron X-ray filaments on the downstream sides, respectively. Here R_s is the radius of the SNR in the unit of pc. From the equation defining $\mathcal{B}$, we obtain

$$D = 0.65 \text{ kpc} \frac{10 \text{ arcsec}}{\theta_d} \left(\frac{\nu_{rolloff}}{10^{17} \text{ Hz}}\right)^{1/2} \left(\frac{\mathcal{B}(t_{age})}{10^{20} \text{ Hz pc}^{-2}}\right)^{-1/2} \quad . \tag{11}$$

The thin solid and dashed lines in Figure 5 represent the relation between the age and the distance using eq.(11), (1), and (2).

On the other hand, $D = R_s/\theta_R$ is rewritten as

$$D = 0.34 \text{ kpc} \frac{10 \text{ arcmin}}{\theta_R} \frac{R_s(t_{age})}{1 \text{ pc}} \quad , \tag{12}$$

$$R_s(t_{age}) = \begin{cases} 1.1 \text{ pc} \left(\frac{E_{51}}{M_{ej}\rho_0} {t_{age}}^4\right)^{1/7} & t < t_{ST} \\ 1.2 \text{ pc} \left(\frac{E_{51}}{\rho_0}\right)^{1/5} \left(t_{age} - 0.22 {E_{51}}^{-1/2} {M_{ej}}^{5/6} {\rho_0}^{-1/3}\right)^{2/5} & t > t_{ST} \end{cases} . \tag{13}$$

The function $R_s(t_{age})$ is given by Truelove & McKee (1999) (see eq.(1) and (2), and table 6 and 7), which studies the shock dynamics of SNRs, where E_{51}, M_{ej}, ρ_0, and t_{ST} is the explosion energy in the unit of 10^{51} ergs, the ejecta mass in the unit of $M_\odot$, the ambient density in the unit of g cm^{-3}, and the time scale that SNRs enter the Sedov-Taylor phase (in which shock begins to deaccelerate due to the interstellar medium), respectively (Truelove & McKee 1999). For simplicity, we consider the case of the constant interstellar medium, n_0,

$$n_0 \equiv \frac{\rho_0}{\mu_H} \tag{14}$$

where μ_H is the mean mass per hydrogen nucleus, $1.4 \times 1.67 \times 10^{-24}$ g. In the following, we choose the kinetic energy of the ejecta, the ejecta mass, and n_0 to be 10^{51} ergs, $1.4M_\odot$, and 0.1 cm^{-3}, respectively. Solving these equations, one can estimate both D and t_{age}.

Figure 5 represents the relation between the age and the distance. We derived the allowed range of the parameters to be

$$t_{age} = 660\ (420 - 1400)\ \mathrm{yrs}\ , \tag{15}$$

$$D = 0.33\ (0.26 - 0.50)\ \mathrm{kpc}\ . \tag{16}$$

When we vary the ambient number density into $n_0 = 0.5$ cm^{-3} or the ejecta mass into $M_{ej} = 10\ M_\odot$, the result remains basically unchanged as can be seen in Figure 5.

Although the allowed regions are too wide to derive some conclusion, we may be able to say that Vela Jr. is a nearby and relatively young SNR. The results are consistent with previous reports, which may imply that this is an indirect confirmation of $\mathcal{B}$—age relation (Bamba et al. 2005) and our distance/age indicator may become a useful tool in the future. Furthermore, derived distance is significantly larger than that of Vela SNR (250 pc; Cha et al. 1999), then there may be no interaction between these two SNRs.

The most common distance indicator of SNR is an application of the relation between the surface brightnesses at 1 GHz and the diameters of SNRs (Σ—D relation; Case & Bhattacharya 1998), however, the relation has still large uncertainties. Recent X-ray surveys recognize a new type of SNRs, which are dim in radio band and bright in hard X-ray band, such as RX J1713.7−3946 (Koyama et al. 1997), G28.6−0.1 (Bamba et al. 2001; Ueno et al. 2003), and so on (e.g. Combi et al. 2005; Yamaguchi et al. 2004). The number of such SNRs may be more than ∼20 (Bamba et al. 2003a). They must be significant accelerators of cosmic rays because most of them emit synchrotron X-rays, Unfortunately, they are dim in radio bands, so that the Σ—D relation cannot directly applied. Our method may also be an useful tool to estimate both D and t_{age} of such synchrotron X-ray emitting SNRs.

Again let us consider E_{max} and B_d using Eqs. (5) and (6). Assuming that $D \sim 300$ pc, that is the most preferable value of our distance indicator, we obtain $E_{max} \sim 3$ TeV and

$B_d \sim 5 \times 10^2$ μG. Although the uncertainty is very large, our result may indicate that the magnetic field is highly amplified.

These results does not include the uncertainty of the model of SNR dynamics and the function $\mathcal{B}$. Considered these uncertainty, the allowed regions for t_{age} and D become more larger. It is the uncertainty of $\mathcal{B}$'s normalization which makes error regions the most widest, about 50%. In order to improve this method for t_{age} and D, more samples are needed to make the uncertainty of $\mathcal{B}$ smaller.

9. Summary

We have conducted systematic spectral and spatial analysis of filamentary structures in Vela Jr. NW rim for the first time. A summary of our results is as follows:

1. We found that nonthermal X-rays from Vela Jr. NW rim are concentrated on very thin filamentary structures. The average scale width on the upstream side is similar to or smaller than the PSF size of *Chandra*, whereas that on the downstream side is 49.5 (36.0–88.8) arcsec.

2. The spectra of filaments are hard and have no line-like structure, which is well reproduced with an absorbed power-law model of $\Gamma = 2.67$ (2.55–2.77), or `SRCUT` model with $\nu_{rolloff} = 4.3$ (3.4–5.3)$\times 10^{16}$ Hz under the assumption of $p = 0.3$.

3. We tried to estimate the distance (D) and the age (t_{age}) of Vela Jr. using the function $\mathcal{B}$ and estimated that $t_{age} = 660$ (420–1400) yrs and $D = 0.33$ (0.26–0.50) kpc, which is consistent with previous reports. These results may suggest that there is no interaction between Vela SNR and Vela Jr.

4. Using the estimated D, we derived the most preferable values $E_{max} \sim 3$ TeV and $B_d \sim 500$ μG. Our result may imply that the magnetic field on the filament is highly amplified.

Our particular thanks are due to the anonymous referee, K. Makishima, F. Takahara, Y. Mochizuki, Y. Moriguchi, Y. Uchiyama, M. Tsujimoto, J. Vink, and K. Ebisawa, for their fruitful discussions and comments. R.Y. and J.S.H. are supported by JSPS Research Fellowship for Young Scientists.

REFERENCES

Aharonian et al. 2005, accepted by A&Aletters (astroph/0505380)

Anders, E., & Grevesse, N. 1989, Geochim. Cosmochim. Acta, 53, 197

Aschenbach, B. 1998, Nature, 396, 141

Bamba, A., Tomida, H., & Koyama, K. 2000, PASJ, 52, 1157

Bamba, A., Ueno, M., Koyama, K., & Yamauchi, S. 2001, PASJ, 53, L21

Bamba, A., Ueno, M., Koyama, K., & Yamauchi, S. 2003a, ApJ, 589, 253

Bamba, A., Yamazaki, R., Ueno, M., & Koyama, K. 2003b, ApJ, 589, 827

Bamba, A. 2004, Ph.D. thesis (Kyoto University)

Bamba, A., Yamazaki, R., Yoshida, T., Terasawa, T., & Koyama, K. 2005, ApJ, 621, 793

Bell, A. R. 1978, MNRAS, 182, 443

Bell, A. R. & Lucek, S. G. 2001, MNRAS, 321, 433

Berezhko, E.G., & Völk, H.J, 2004, A&A, 419, L27

Blandford, R. D., & Eichler, D. 1987, Phys. Rep., 154,1

Borkowski, K. J., Rho, J., Reynolds, S. P. & Dyer, K. K. 2001, ApJ, 550, 334

Blandford, R. D., & Ostriker, J. P. 1978, ApJ, 221, L29

Burgess, C. P. & Zuber, K. 2000, Astroparticle Physics, 14, 1

Case, G. L., & Bhattacharya, D. 1998, ApJ, 504, 761

Cassam-Chenaï, G., Decourchelle, A., Ballet, J., Sauvageot, J.-L., Dubner, G., & Giacani, E. 2004, A&A, 427, 199

Cha, A. N., Sembach, K. R., & Danks, A. C. 1999, ApJ, 515, L25

Combi, J. A., Romero, G. E., & Benaglia, P. 1999, ApJ, 519, L177

Combi, J.A., Benaglia, P., Romero, G.E., & Sugizaki, M. 2005, A&A, in press (astroph/0501051)

Drury, L.O'C. 1983, Rep. Prog. Phys., 46, 973

Fukui, Y., et al. 2003, PASJ, 55, L61

Garmire, G., Feigelson, E. D., Broos, P., Hillenbrand, L. A., Pravdo, S. H., Townsley, L.,& Tsuboi, Y. 2000, AJ, 120, 1426

Green, D. A. 2004, A Catalogue of Galactic Supernova Remnants (2004 January version), (Cambridge, UK, Mullard Radio Astronomy Observatory) available on the WWW at http://www.mrao.cam.ac.uk/surveys/snrs/

Hiraga, J. S., et al. 2005, ApJ, submitted

Hwang, U., Decourchelle, A., Holt, S. S., & Petre, R. 2002, ApJ, 581, 1101

Iyudin, A. F., et al. 1998, Nature, 396, 142

Iyudin, A. F., Aschenbachm B., Becker, W., Dennerl, K., & Haberl, F. 2005, A&A, 429, 225

Jones, F.C., & Ellison, D.C. 1991, Space Science Rev., 58, 259 ApJ, 580, 1060

Katagiri, H. et al. 2005, ApJ, in press (astro-ph/0412623)

Koyama, K., Kinugasa, K., Matsuzaki, K., Nishiuchi, M., Sugizaki, M., Torii, K., Yamauchi, S., & Aschenbach, B. 1997, PASJ, 49, L7

Koyama, K., Petre, R., Gotthelf, E.V., Hwang, U., Matsura, M., Ozaki, M., & Holt S. S. 1995, Nature, 378, 255

Lazendic, J. S., Slane, P. O., Gaensler, B. M., Reynolds, S. P., Plucinsky, P. P., & Hughes, J. P. 2004, ApJ, 602, 271

Long, K. S., Reynolds, S. P., Raymond, J. C., Winkler, P. F., Dyer, K. K., & Petre, R. 2003, ApJ, 586, 1162

Lucek, S. G. & Bell, A. R. 2000, MNRAS, 314, 65

Malkov, E., & Drury, L.O'C. 2001, Rep. Prog. Phys., 64, 429

Mereghetti, S., Pellizzoni, A., & de Luca, A. 2002, ASP Conf. Ser. 271: Neutron Stars in Supernova Remnants, 289

Moriguchi, Y., Yamaguchi, N., Onishi, T., Mizuno, A., & Fukui, Y. 2001, PASJ, 53, 1025

Morrison, R., & McCammon, D. 1983, ApJ, 270, 119

Pavlov, G. G., Sanwal, D., Kızıltan, B., & Garmire, G. P. 2001, ApJ, 559, L131

Reynolds, S. P. 1998, ApJ, 493, 375

Reynolds, S.P., & Keohane, J.W. 1999, ApJ, 525, 368

Rho, J., Dyer, K. K., Borkowski, K. J., & Reynolds, S. P. 2002, ApJ, 581, 1116

Shonfelder, V., et al. 2000, in AIP Conf. Proc. 510, Fifth Compton Symp., ed. M. L. McConnell & J. M. Ryan (New York: AIP), 54

Slane, P., Gaensler, B. M., Dame, T. M., Hughes, J. P., Plucinsky, P. P., & Green, A. 1999, ApJ, 525, 357

Slane, P., Hughes, J. P., Edgar, R. J., Plucinsky, P. P., Miyata, E., Tsunemi, H., & Aschenbach, B. 2001, ApJ, 548, 814

Truelove, J. K., & McKee, C. F. 1999, ApJS, 120, 299

Tsunemi, H., Miyata, E., Aschenbach, B., Hiraga, J., & Akutsu, D. 2000, PASJ, 52, 887

Uchiyama, Y., Aharonian, F. A., & Takahashi, T. 2003, A&A, 400, 567

Ueno, M., Bamba, A., Koyama, K., & Ebisawa, K. 2003, ApJ, 588, 338

Vink, J. & Laming, J. M. 2003, ApJ, 584, 758

von Keinlin, A., Atté, D., Schanne, S., Cordier, B., Diehl, R., Iyudin, A. F., Lichti, G. G., Roques, J. -P., Schönfelder, V., & Strong, A. 2004, Proc. of the 5th *INTEGRAL* Science Workshop, ESA SP-552 (astrpph/0407129)

Weisskopf, M. C., Brinkman, B., Canizares, C., Garmire, G., Murray, S., & Van Speybroeck, L. P. 2002, PASP, 114, 1

Yamaguchi, H., Ueno, M., Koyama, K., Bamba, A., & Yamauchi, S. 2004, PASJ, 56, 1059

Yamazaki, R., Yoshida, T., Terasawa, T., Bamba, A., & Koyama, K. 2004, A&A, 416, 595

This preprint was prepared with the AAS LaTeX macros v5.2.

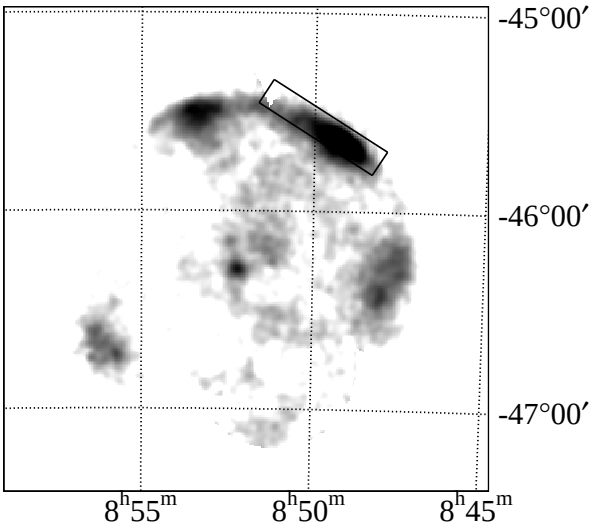

Fig. 1.— *ASCA* GIS image of Vela Jr. in the 0.7–10.0 keV band (Tsunemi et al. 2000). Gray-scale is in logarithmic and coordinates are in J2000. The solid rectangle shows the field of view of *Chandra* ACIS-S array.

Table 1. Observation Log

ObsID	R.A.	Dec.	Date	Exposure (ks)
3846	$08^{h}49^{m}09^{s}.3$	$-45^{d}37^{m}42^{s}.4$	2003 Jan. 5	39
4414	$08^{d}49^{m}09^{s}.3$	$-45^{d}37^{m}42^{s}.3$	2003 Jan. 6	35

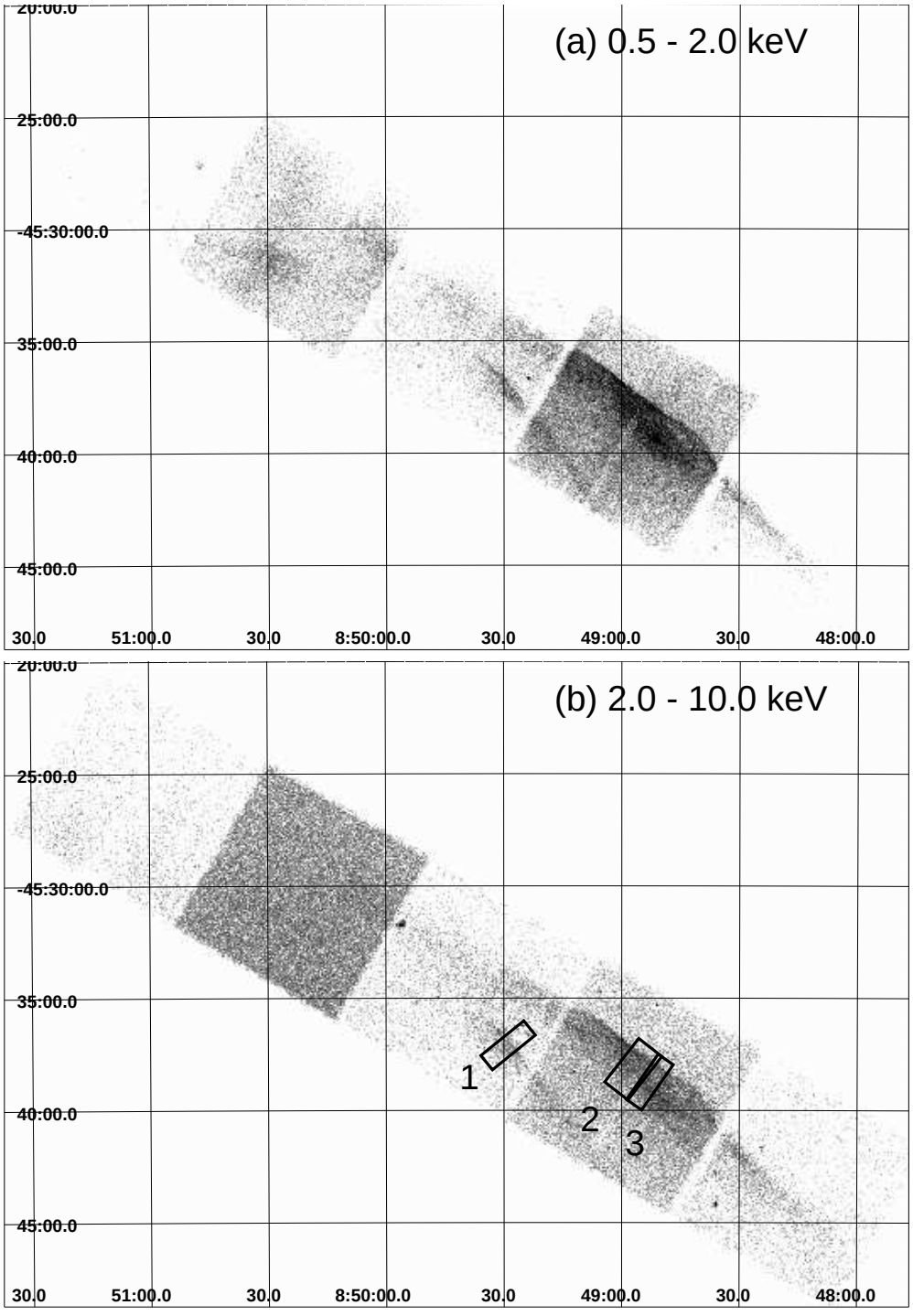

Fig. 2.— *Chandra* images of the NW rim of Vela Jr. in the 0.5–2.0 keV band (a) and 2.0–10.0 keV band (b). Gray-scales are in logarithmic and coordinates are in J2000, binned with 4 arcsec scale. Regions to make profiles are shown in (b) with solid rectangles.

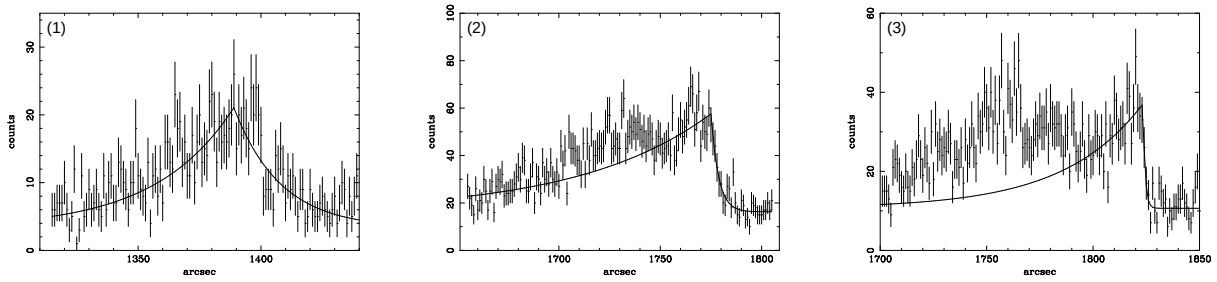

Fig. 3.— Profiles of the filaments in the 2.0–10.0 keV band, binned with 1 arcsec scale. The best-fit models are shown with solid lines. In each panel, the shock runs from left to right. For filaments 2 and 3, each fitting was carried out only around the outer peak in order to avoid the contamination from the inner peak.

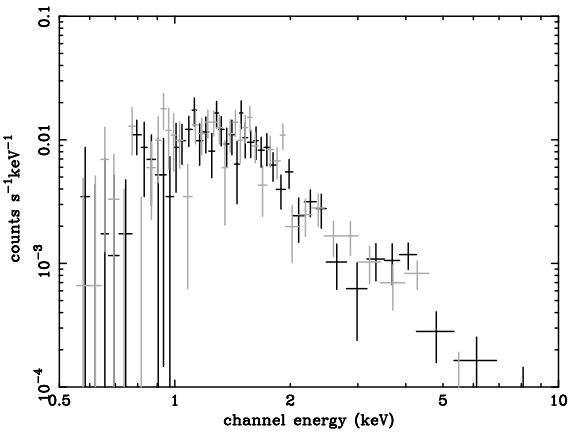

Fig. 4.— Spectra of the filament 1. The black and gray data set represent the data for obsID = 3846 and 4414, respectively.

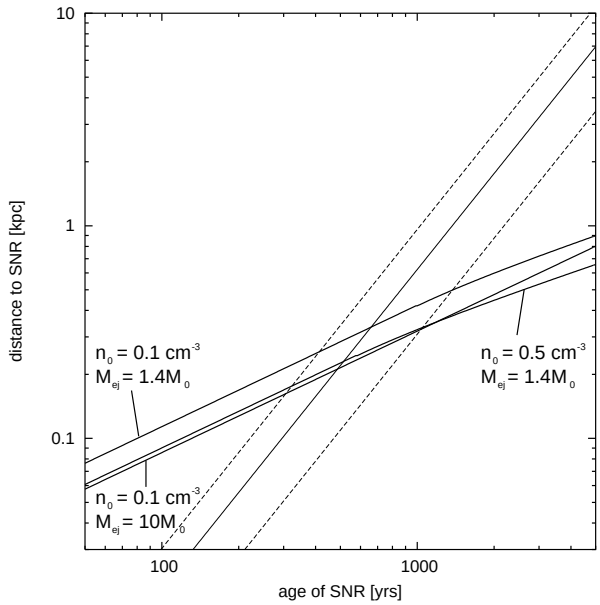

Fig. 5.— The relations between the age and the distance derived from the evolution of SNRs and from the function $\mathcal{B}$. The bold, solid, and dashed lines are the relations from the SNR model, and best-fit one from the function $\mathcal{B}$ and their allowed regions, respectively.

Table 2. Best-fit parameters of the Spectrum of the NW rim[a]

Parameters	Best-Fit Value
Γ	2.67 (2.52–2.84)
$N_{\rm H}$ $[10^{21}$ H cm$^{-2}]$[b]	6.1 (2.4–9.9)
Flux[c] $[10^{-12}$ergs cm^{-2}s$^{-1}]$.	6.2 (5.9–6.5)
χ^2/d.o.f.	114.4/135

[a]Parentheses indicate single parameter 90% confidence regions.

[b]Calculated using the cross sections by Morrison & McCammon (1983) with the solar abundances (Anders & Grevesse 1989).

[c]In the 2.0–10.0 keV band.

Table 3. Best-fit parameters of the profiles of the filaments.[a]

No.	A [cnts arcsec^{-1}]	w_u [arcsec]	w_d [arcsec]	Reduced χ^2 [χ^2/d.o.f.]
1.....	17.8 (15.8–19.9)	19.0 (12.1–31.4)	31.8 (23.7–47.1)	143.4/121
2.....	41.4 (36.5–47.4)	3.68 (2.69–5.75)	65.0 (38.2–144.6)	56/51
3.....	26.4 (22.4–30.7)	··· [b]	37.1 (26.5–60.2)	58/54
mean[c] ..	···	···	49.5 (34.8–98.3)	···

[a]Parentheses indicate single parameter 90% confidence regions.

[b]Fixed to be 1 arcsec.

[c]Flux-weighted mean value.

Table 4. Best-fit parameters of the spectra of the filaments.[a]

	`power-law`			`srcut` ($p = 0.3$)			`srcut` ($p = 0.5$)		
No.	Γ	Flux[b]	χ^2/d.o.f.	$\nu_{rolloff}$[c]	$\Sigma_{1\mathrm{GHz}}$[d]	χ^2/d.o.f.	$\nu_{rolloff}$[c]	$\Sigma_{1\mathrm{GHz}}$[d]	χ^2/d.o.f.
1.....	2.87	0.74	76.2/81	2.7	4.4	79.2/81	3.7	148	76.1/81
	(2.71–3.06)	(0.63–0.85)		(1.8–3.8)	(2.8–3.8)		(2.6–5.8)	(95–230)	
2.....	2.59	1.8	137.3/118	5.3	1.2	141.3/118	8.2	120	141.3/118
	(2.44–2.74)	(1.6–2.1)		(3.6–7.3)	(1.1–1.3)		(5.5–12.8)	(113–127)	
3.....	2.45	0.76	56.2/44	7.4	0.93	57.7/44	11.6	32	57.4/44
	(2.23–2.68)	(0.61–0.92)		(4.1–13.2)	(0.84–1.01)		(6.4–25.7)	(28–36)	
Total.	2.67	3.2	276.8/245	4.3	8.8	286.6/245	6.6	282	284.9/245
	(2.57–2.77)	(2.9–3.6)		(3.4–5.3)	(8.1–9.5)		(5.0–8.7)	(262–301)	

Note. — The absorption column was fixed to be 6.1×10^{21} H cm^{-2} according to Table 2.

[a]Parentheses indicate single parameter 90% confidence regions.

[b]Absorption-corrected flux in the 2.0–10.0 keV band in the unit of 10^{-13} ergs cm^{-2}s^{-1}.

[c]Roll-off frequency in the unit of 10^{16} Hz.

[d]Flux density at 1 GHz in the unit of 10^{-4} Jy.